Fermi National Accelerator Laboratory

FERMILAB-Pub-92/136
TM-1774

# Pre-conceptual Design of a Proton Therapy Accelerator

C. Ankenbrandt, T. Kroc, L. Michelotti, S. Peggs, and C. Schmidt

*Fermi National Accelerator Laboratory*
*P.O. Box 500, Batavia, Illinois 60510*

May 1992

Operated by Universities Research Association Inc. under Contract No. DE-AC02-76CHO3000 with the United States Department of Energy

## Disclaimer

*This report was prepared as an account of work sponsored by an agency of the United States Government. Neither the United States Government nor any agency thereof, nor any of their employees, makes any warranty, express or implied, or assumes any legal liability or responsibility for the accuracy, completeness, or usefulness of any information, apparatus, product, or process disclosed, or represents that its use would not infringe privately owned rights. Reference herein to any specific commercial product, process, or service by trade name, trademark, manufacturer, or otherwise, does not necessarily constitute or imply its endorsement, recommendation, or favoring by the United States Government or any agency thereof. The views and opinions of authors expressed herein do not necessarily state or reflect those of the United States Government or any agency thereof.*

Interest has now turned to the design and use of dedicated facilities optimized for radiation therapy. Fermilab was heavily involved in the design and implementation of the first such hospital-based synchrotron, the machine at Loma Linda University Medical Center. Given Fermilab's history of contributions to proton therapy as well as the successful experience with the Neutron Therapy Facility at Fermilab, it is natural for Fermilab scientists to turn once again to the design and development of particle therapy facilities. That task involves choosing among available technologies and optimizing the relevant parameters to meet the medical requirements and maximize the ratio of medical capabilities to costs. The following sections describe the resulting design in some detail; it is appropriate in the rest of this section to expose the rationale for the more important design decisions and to highlight the major features of the facility.

General desiderata for a therapy accelerator are discussed first because such considerations motivate subsequent design choices. Besides the obvious requirement to deliver beam of the appropriate characteristics, preeminent design goals of a medical accelerator include reliability, economy, ease of maintenance, and patient safety.[3] Contrast the design of high energy physics (HEP) research accelerators, where ultimate performance is commonly desired along with low capital cost. Beam users at a HEP laboratory are prepared to tolerate relatively frequent data taking interruptions, not only because that is the price of high performance but also because many technically skilled people are ready to effect repairs quickly. The manager of a medical radiation facility can not be so tolerant - only very infrequent rescheduling of patient treatment is acceptable and considerably fewer maintenance people are on site. Furthermore, although personnel safety is heavily emphasized at HEP facilities, additional safety measures are necessary in a facility where patients are deliberately exposed to beam.

The design of the Proton Therapy Accelerator (PTA) therefore emphasizes simplicity and modularity, for example by minimizing the number of different component types so that many parts are interchangeable. The PTA design is also conservative in that the technologies adopted are well-established by successful use at existing accelerators. Furthermore, the design specifications are far from performance limits; the conservative methods used to estimate the performance limits have been validated by experience with other accelerators.

We turn now to an exposition of specific design choices for the PTA, of which the first is the particle type. Although higher-Z particles have marginal advantages over protons (smaller deviations from their original trajectories due to multiple scattering and higher energy loss per unit path length or linear energy transfer), protons are chosen because for a given range in matter proton accelerators are considerably smaller and less expensive than accelerators for heavier ions.

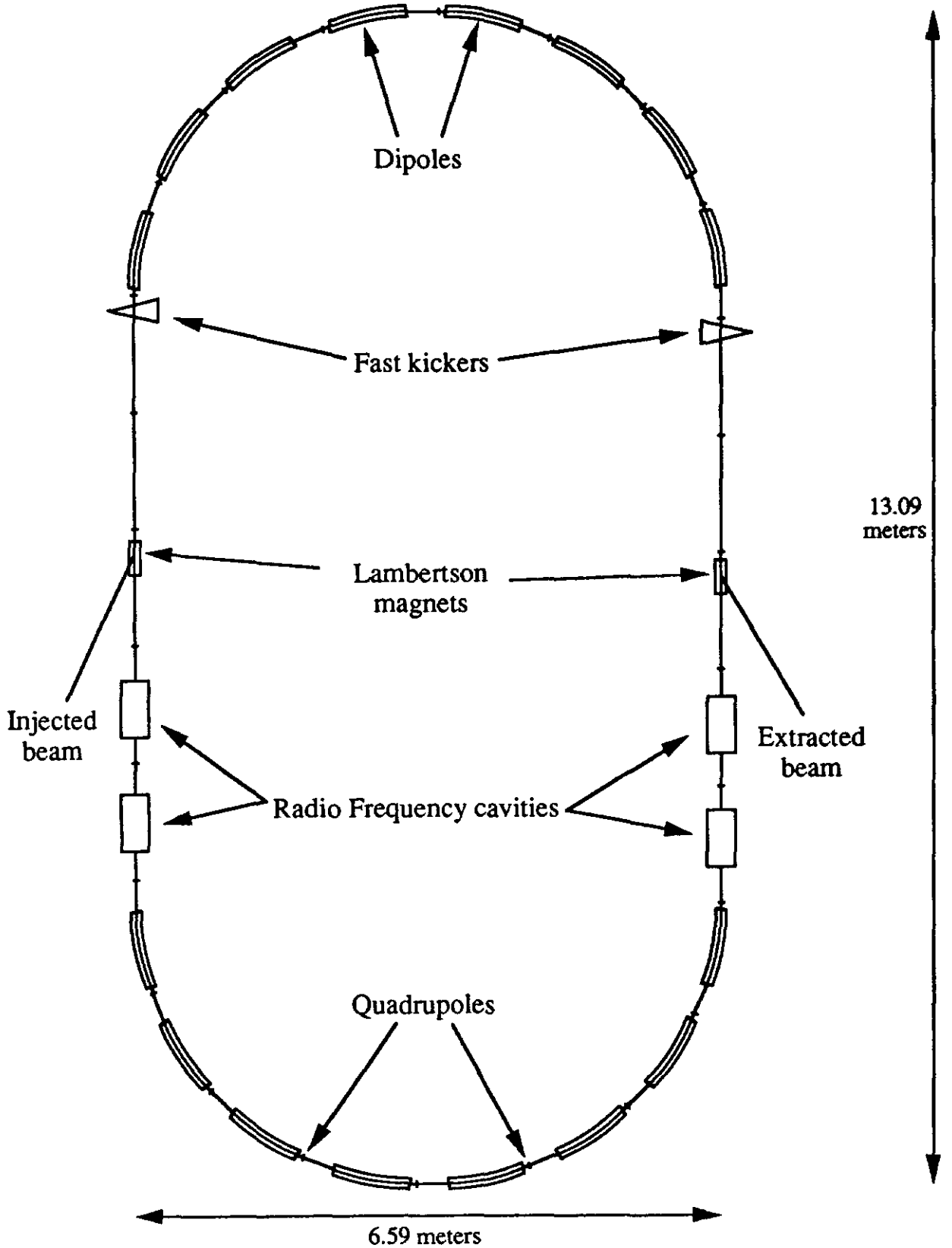


Figure 1.1 Schematic of the racetrack layout of the PTA synchrotron

Similarly, we choose to start with protons rather than $H^-$ ions because the technologies of proton sources and injection methods are simpler than those of $H^-$ ions and the characteristic features that $H^-$ ions provide are not needed.

We believe that a synchrotron is the machine of choice for proton therapy. The most significant advantage over a linac or a cyclotron is that an appropriately designed synchrotron can straightforwardly produce a beam whose output energy is continuously variable within wide limits, a capability necessary for the beam delivery concepts to be described below. Linacs and cyclotrons can produce more intense beams, but a well-designed synchrotron can easily provide enough beam intensity for a therapy facility. The cost of a synchrotron is probably less than that of a linac and comparable to that of a cyclotron.[4]

The proton synchrotron incorporates three features that are most important to achieving the design goals of the PTA:

*1) <u>The optical lattice is made from FODO cells</u>. That is, the magnet distribution or lattice includes regularly spaced quadrupoles that alternately focus and defocus the beam; one period of this repetitive structure includes one quadrupole of each polarity and is called a FODO cell. This is the simplest realization of the alternating gradient concept, which results in strong net focusing in both transverse directions. The space between quadrupoles is either magnetically empty, or is (almost) filled with a single bending dipole. Straight and bending half cells are assembled to make the racetrack layout that is shown in Figure 1.1. FODO optics are extremely simple and well behaved, with tight focusing that reduces the horizontal and vertical beam sizes, thereby reducing the costs of magnets because their transverse sizes can be small. Only one kind of dipole and one kind of quadrupole are necessary. One power supply runs all dipoles and quadrupoles in the ring.*

*2) <u>The synchrotron is rapid-cycling and uses single-turn extraction</u>. Beam can be extracted from a synchrotron using single-turn fast extraction or resonant slow spill; fast extraction is preferable for several reasons. The minimal hardware and controls necessary to achieve single-turn extraction lead to a simpler and more robust system than that necessary to achieve slow extraction over thousands of turns. Furthermore, the beam can be fast-extracted at arbitrary energy simply by changing the firing time of the extraction kicker; (of course the strengths of extraction kicker, septum, and beam transport elements must be changed to track the beam momentum). Slow extraction inherently generates beam losses of order 1% or more, whereas fast extraction is inherently "clean". Unlike slow spill, fast extraction imposes no special requirements on the good-field aperture at extraction time. Painting the beam over a tumor*

*volume during slow spill requires uniform spill; it is hard in practice to avoid fluctuations of the order of ten per cent in the spill rate of slowly extracted beam.*

*Fast extraction allows the choice of a rapid-cycling synchrotron; slow spill takes so long that it effectively precludes rapid-cycling. A slow cycle essentially demands that a lot of protons occupy the accelerator simultaneously in order to achieve acceptable treatment times; slow extraction thus carries the threat of suddenly dumping a lot of beam into a localized region of a patient. A fast repetition rate allows the intensity requirements to be met with modest intensities per cycle, thereby eliminating intensity-dependent problems such as coherent instabilities and space-charge effects. It also allows scanning of large tumor volumes by delivering one beam bunch to each volume element or "voxel," creating the desired dose distribution throughout the tumor while minimizing the dose delivered to normal tissue. This beam delivery method, which we call "pointillism," seems to be the most promising approach to realizing the full potential of proton therapy. Eros Pedroni and coworkers at PSI have developed a similar approach to beam delivery.[5] The high level of repeatability that comes with rapid cycling provides a natural way to ensure delivery of the intended number of protons on each cycle: if the accelerated beam falls outside tight intensity specifications, then it is trivial to reject that cycle and wait for the next, in order to continue a scan of the patient. In this sense the PTA is a "digital" treatment accelerator. Finally, rapid cycling significantly reduces power costs, as shall be discussed below.*

*It is worth noting in passing that the 500 MeV rapid cycling proton booster at the KEK high energy laboratory in Japan bears some similarities to the PTA. For several years now it has used parasitic beam to treat a modest number of patients.[6]*

*3) <u>Beam is injected at a kinetic energy of 15 MeV</u>. The use of a relatively high injection energy bestows several advantages. It makes the protons more dynamically "rigid", significantly ameliorating the effect of the electrostatic "space charge" forces attempting to disrupt the bunch. In conjunction with the relatively small beam intensity per cycle, this means that space charge effects are negligible. Also, since the beam shrinks adiabatically as it accelerates, a higher injection energy makes for a smaller beam, reducing the required synchrotron aperture. Higher injection momentum means stronger magnetic fields at injection time, reducing the effects of remanent fields. An injection energy of 15 MeV reduces the required frequency swing of the rf system to less than a factor of four, permitting the use of resonant radio frequency cavities for acceleration rather than broad-band structures. Finally, an energy of 15 MeV is high enough to produce many biologically significant radioisotopes.*

*A partial list of the high energy proton machines whose injection energies have been or are being raised to improve their performance includes the Fermilab Booster, the Brookhaven AGS (twice), and the CERN PS. The designers of other machines, such as the Fermilab Tevatron, insisted upon high injection energies from the start. Iteration of the SSC design has resulted in raising the design injection energies of most of the rings. There is no doubt that the community has arrived at the consensus that high injection energies are valuable.*

A maximum kinetic energy of 250 MeV, corresponding to a range of about 38 cm in water-equivalent tissue, is generally considered sufficient for proton therapy because it allows the beam to penetrate most of the way through most human bodies in any direction perpendicular to the long axis. However, we choose a higher energy, 300 MeV, corresponding to a range of about 51 cm in water-equivalent tissue, in order to facilitate proton computed tomography, which requires penetration all the way through the body. (Proton CT is like X-ray CT except that the images are based not on X-ray attenuation measurements but on measurements of proton energy loss or residual range for multiple trajectories through the body.) The 20% change in kinetic energy increases the range by 33% while raising the maximum beam momentum by 11% and the size of the synchrotron by only 6%; hence the cost impact is modest.

It has been shown that proton computed tomography can produce medical images of quality comparable to conventional X-ray CT machines while delivering significantly lower doses.[7] Although it is probably futile to try to compete with the large installed base of existing X-ray CT facilities for general medical imaging applications, the ability to acquire high-quality images quickly using the same beam and with the patient positioned in the same way as for treatment would be a significant addition to the capabilities of future proton therapy facilities and may well become an important aspect thereof. Such images would be very useful for verifying correct patient positioning; the ability to monitor changes that may occur during the course of treatment could also prove valuable. Developing these capabilities represents an interesting research opportunity at the facility described here.

In various workshops on proton therapy, an average beam intensity of about $10^{11}$ protons per second has generally been deemed sufficient to supply the needs of a large therapy facility. Although this is small compared to the intensities achieved by some synchrotrons for high-energy physics, still it is not trivial to achieve in a small synchrotron with a low injection energy. The intensity requirement is "soft" in the sense that the highest intensities are needed only occasionally, mainly to treat large tumors in reasonable times (generally in exposure times of order a minute per visit), and the needs are sometimes inflated by allowing for various inefficiencies, especially the

losses which inevitably accompany passive beam-spreading techniques. Nevertheless, the PTA has been designed to achieve a higher intensity, at least $3\times10^{11}$ protons per second. The most important consequence of the high design intensity may be that no intensity dependence of accelerator performance or beam sizes will be encountered in everyday operation as the intensity is adjusted over a range of values well below the ultimate performance limit. Higher intensities may also prove valuable for marginally shortening treatment times and/or for supplying beam to additional treatment rooms in the future; the intensity limitations of the accelerator should not unnecessarily constrain the size of tumor that can be treated or the scope of the facility.

| Property | units | Value |
|---|---|---|
| Injection kinetic energy | MeV | 15 |
| Maximum extraction kinetic energy | MeV | 300 |
| Repetition rate, $f_{rep}$ | Hz | 30 |
| Protons per pulse | | $10^{10}$ |
| Circumference | m | 33.8 |
| Half cell length | m | 1.3 |
| Number of dipoles | | 16 |
| Number of quadrupoles | | 26 |
| Number of sextupoles | | 10 |

Table 1.1 Primary parameters of the Proton Therapy Accelerator.

Space requirements for the medical synchrotron itself (as opposed to the beam delivery system) are not critical. Table 1.1, which displays general PTA parameters, shows that the circumference of the PTA is 33.8 meters. The footprint area that this requires is not a significant fraction of the total area of the treatment facility. Although the circumference probably could be reduced by several percent by packing magnetic elements more closely together, it would be folly to do so, because installation and maintenance difficulties would ensue. At the same time, there is not much money to be saved (if any) by reducing the circumference since the total length of dipole magnets - the most costly magnetic component - depends only on the maximum allowed field. In contrast, a careful design of the beam delivery system can result in big cost savings. Continuing in

the spirit of emphasizing simplicity, we suggest horizontal beam delivery to a standing or sitting patient whenever possible, and present the design of a flexible and cost efficient horizontal delivery line below.

Sections 2, 3, and 4 contain descriptions of the injection system, the synchrotron lattice and layout, and the radio frequency acceleration system, respectively. Section 5 addresses beam delivery and patient treatment planning issues and presents economical and flexible designs for a beam transport line and a nozzle delivery system.

# 2. Injection linac system

The 15-MeV injector for the proton therapy synchrotron is shown schematically in Figure 2.1. It is a conventional system composed of a proton source, a radio frequency quadrupole linac (RFQ), an Alvarez type drift tube linac (DTL), and intermediate beam transport systems.

Short beam pulses of low current at a repetition rate of 30 Hz furnish more than enough protons to satisfy the modest intensity requirements of proton therapy; for example, the synchrotron design intensity corresponds to injected beam of 16 mA for 100 nsec or 3.2 mA for 500 nsec. However, it is desirable to preserve the possibility of using the same injector to support other medical programs of high current interest, such as boron neutron capture therapy (BNCT) and positron emission tomography (PET). Accordingly, the injector described here is able to supply high currents and long pulses at a repetition rate of 60 Hz in order to provide the high average proton currents required by such programs. (BNCT requires average currents of a few mA at a few MeV; at 15 MeV, an average current of 1 mA should be sufficient. Isotope production for PET does not need as much intensity.) The incremental cost of augmenting the intensity capability of the linac is relatively modest. Various simple schemes can be envisioned downstream of the DTL to share beam between the synchrotron and other facilities.

### Ion Source

The source is a conventional duoplasmatron proton ion source. The duoplasmatron is a very reliable well-understood source capable of high proton intensities (>200 mA) and high duty factor. To achieve the high currents, the source will be at high potential (100 kV) and accelerate protons to ground through a short transport line into the RFQ.

Two types of transport line from the source to the RFQ are under consideration. A standard source transport line would be composed of two magnetic solenoid lenses to achieve the strong focusing to match into the RFQ. This line would be about one meter long. Gas neutralization

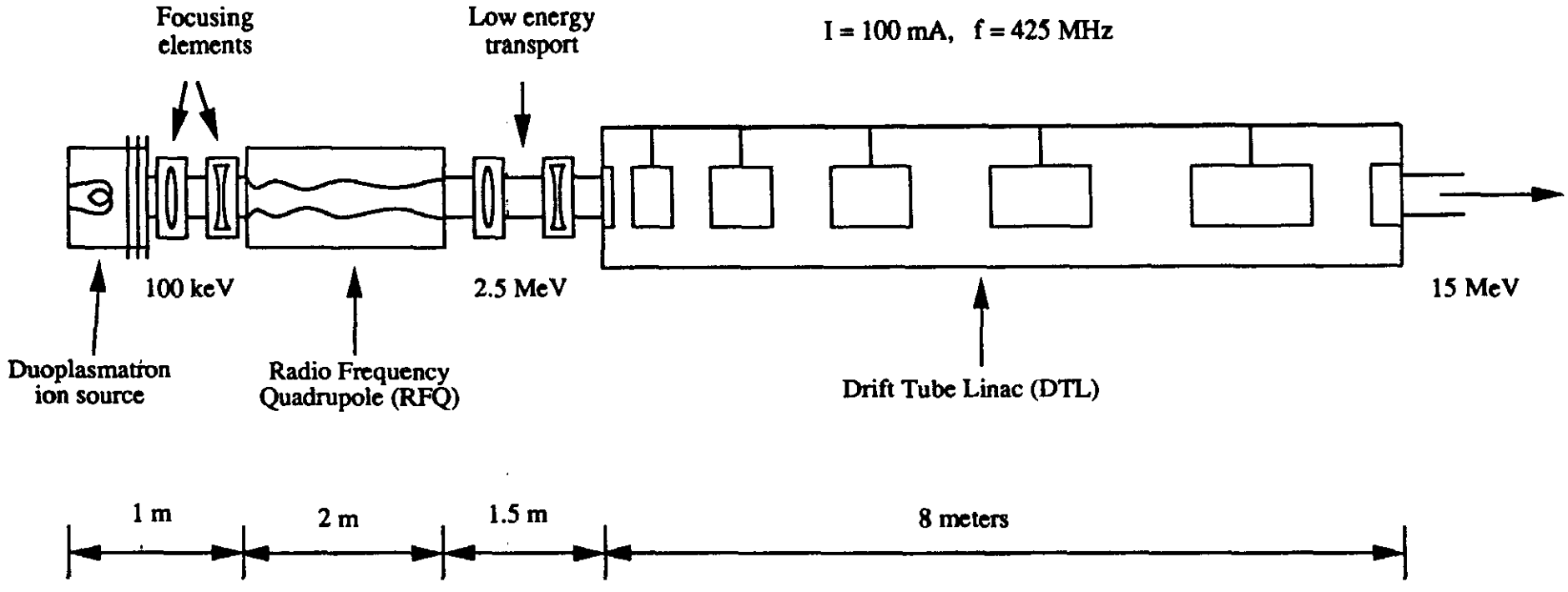


Figure 2.1 Schematic drawing of the 15 MeV linac injector

would be needed to compensate for space charge forces in the beam at high intensity, but this would also produce undesirable time dependence of the beam parameters until the ion distribution reaches equilibrium. These changes, having time constants of ten or more microseconds, cause significant phase space rotations at the beginning of the pulse and a mismatch into the RFQ. Alternate transport lines would use electrostatic lenses to prevent beam neutralization, thereby avoiding the associated time dependence of beam parameters. Depending on the beam current, these focusing devices could be high voltage einzel lenses or new types of electrostatic quadrupole lenses. The electrostatic line is typically shorter and better preserves the beam quality but is more complex.

### Radio-frequency Quadrupole Linac

The radio-frequency quadrupole linac (RFQ) accelerates protons to an energy of approximately 2.5 MeV. It is a standard vane RFQ operating at a frequency of 425 MHz. With an injection energy of 100 keV, a high beam current is achievable[8]; 100 mA at 1% duty factor is called for. Matching from the RFQ to the drift tube linac (DTL) is facilitated by closely coupling the RFQ to the DTL.

### Drift Tube Linac

The final part of the injector is a 15-MeV Alvarez type DTL operating at the RFQ frequency of 425 MHz. For the purposes of the synchrotron, which requires short pulses of low intensity, the injector is rather conservative. For BNCT the requirements of high current (~100 mA) and high duty-factor (~1%) are more difficult, but they have been achieved in normal operation at other facilities.

From past experience, a typical normalized transverse root mean square emittance, $\varepsilon$, from the source is 0.5 μm. From the RFQ it may be 0.7 μm and from the DTL it should be less than 1 μm in both transverse planes. The longitudinal emittance of individual micro-bunches from the linac is basically irrelevant for the synchrotron because many linac bunches are captured in a single bucket in the synchrotron. The longitudinal emittance of the synchrotron beam is determined by the product of the total momentum spread and the pulse length of the linac beam. The expected total fractional momentum spread dp/p of $10^{-3}$ and a pulse duration of 500 nsec imply a total area in longitudinal phase space of less than 0.02 eV-sec.

Table 2.1 contains major parameters of the injection system.

| Property | units | Value |
|---|---|---|
| **Duoplasmatron Ion Source** | | |
| Output energy | MeV | 0.10 |
| Pulse rate | Hz | 30 - 60 |
| Duty factor | % | 1 |
| **Radio Frequency Quadrupole (RFQ)** | | |
| Output energy | MeV | 2.5 |
| Frequency | MHz | 425 |
| Length | m | 2.0 |
| **Drift Tube Linac (DTL)** | | |
| Proton current | mA | 100 |
| Output energy | MeV | 15.0 |
| Frequency | MHz | 425 |
| Length | m | 8.0 |
| Total momentum width, $\Delta p/p$ | | $1.0 \times 10^{-3}$ |

Table 2.1 Parameters of the linac injection system into the PTA synchrotron.

# 3. Synchrotron Layout and Lattice

Figure 1.1 shows the racetrack footprint of the PTA synchrotron, consisting of two straight sections and two 180 degree bend sections or arcs. Each straight section consists of five FODO half cells without dipoles and each arc consists of eight half cells with dipoles. The distance from one quadrupole to the next is the total half cell length, 1.3 meters. With a grand total of 26 half cells, the total circumference of the PTA is 33.8 meters. Between the quadrupoles in each bending half cell is one rectangular dipole 0.88 meters long with a maximum field of 1.2 Tesla. Each of the 16 dipoles bends the beam through 22.5 degrees. Rectangular dipoles - with parallel end faces - are used instead of sector dipoles because they can be constructed by the simple method of stacking

laminations parallel vertically on a jig that curves by 22.5 degrees horizontally to follow the beam trajectory. More information about the magnets and other aspects of the synchrotron lattice can be found in Table 3.1.

| Property | units | Value |
|---|---|---|
| Injection momentum | GeV/c | 0.168 |
| Maximum extraction momentum | GeV/c | 0.808 |
| Maximum horizontal beta function, $\beta_{x\,max}$ | m | 4.0 |
| Maximum vertical beta function, $\beta_{y\,max}$ | m | 5.8 |
| Maximum dispersion function, $\eta_{max}$ | m | 2.6 |
| Phase advance per cell, horizontal and vertical | degrees | 90 |
| Horizontal tune, $Q_x$ | | 3.25 |
| Vertical tune, $Q_y$ | | 3.25 |
| Normalized root mean square emittance, $\varepsilon$ | m | $1.0 \times 10^{-6}$ |
| Momentum width at injection, $\sigma_p/p$ | | $3.0 \times 10^{-4}$ |
| Maximum rms beam height (15 MeV) | mm | 5.7 |
| Maximum rms betatron beam width (15 MeV) | mm | 4.7 |
| Maximum rms momentum beam width (15 MeV) | mm | 0.8 |
| Maximum rms total beam width (15 MeV), $\sigma_x$ | mm | 4.8 |
| Magnetic length of dipole | m | 0.88 |
| Maximum dipole field (300 MeV) | Tesla | 1.2 |
| Magnetic length of quadrupole | m | 0.14 |
| F quadrupole gradient (300 MeV) | Tesla/m | 21.6 |
| D quadrupole gradient (300 MeV) | Tesla/m | 19.5 |

Table 3.1 Optical and other parameters of the PTA synchrotron.

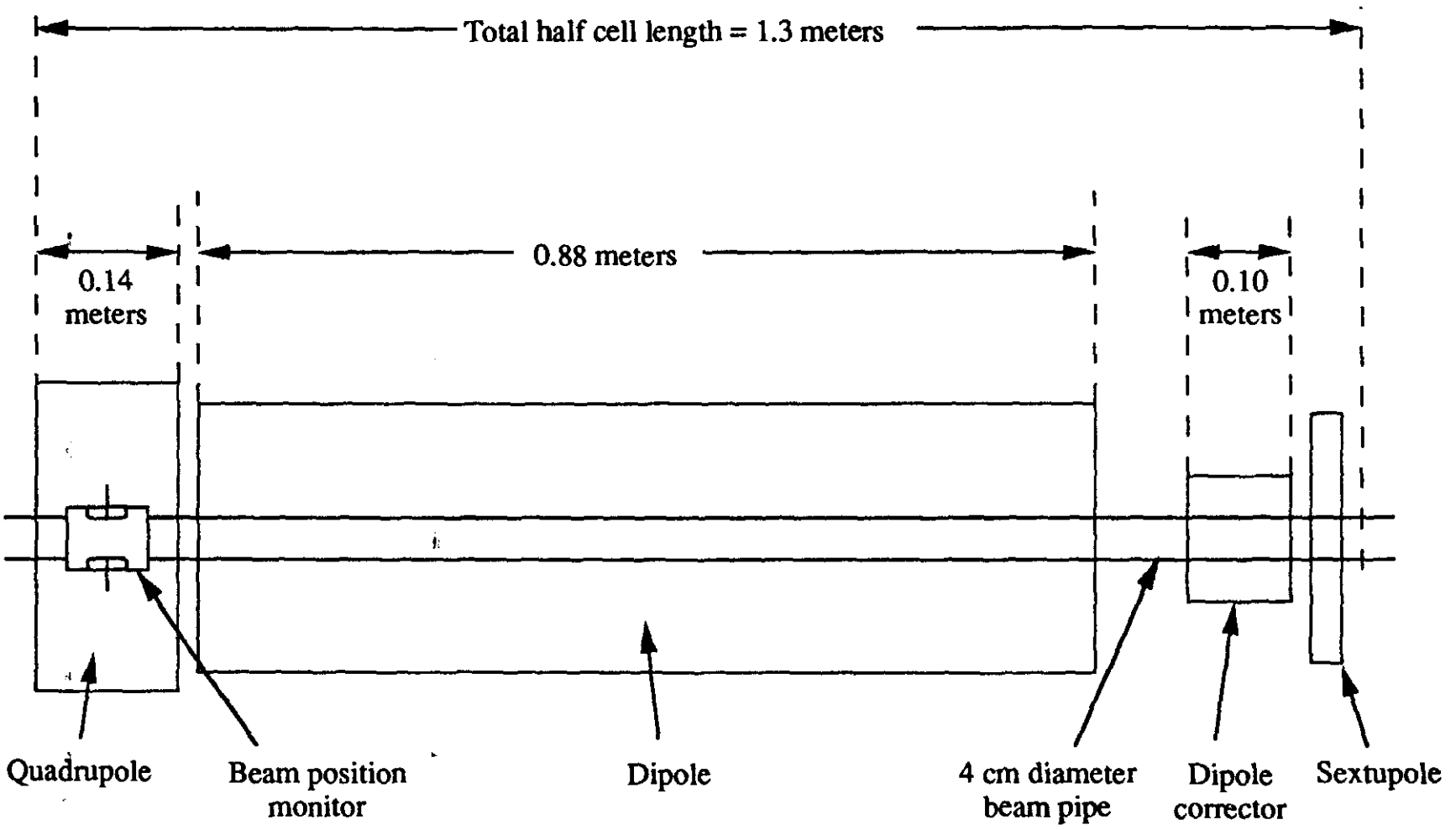


Figure 3.1 Layout of a bending half cell, including a sextupole corrector. Side view, approximately to scale.

Figure 3.1 illustrates the layout of a bending half cell, including a quadrupole, a dipole, a Beam Position Monitor (BPM), a dipole corrector, and a sextupole. (One of the design goals was to reduce the number of different component types. The chosen lattice has only one kind of each of these elements. This minimizes the effort devoted to component design and development and reduces the required inventory of spares.) The dipole is placed as far upstream as possible to maximize the free space available between its downstream end and the next quadrupole. The BPM is integrated into the vacuum pipe in the center of the PTA quadrupoles, a configuration copied from the corresponding components developed for the Fermilab linac upgrade. Since PTA energies are comparable with Fermilab linac energies, it is not surprising that the specifications of their quadrupoles are quite similar. It might even be possible to use Fermilab linac quadrupole laminations in the PTA quadrupoles. Similarly, it might be possible to use Fermilab linac dipole correctors in the PTA, after a relatively modest redesign. Sextupoles are included only at those locations where the horizontal dispersion function is large, for a total of five sextupoles per arc.

Figure 3.2 shows the optical functions - the beta functions $\beta_x$ and $\beta_y$ and the horizontal dispersion $\eta$ - for the PTA synchrotron. These quantities are related to the horizontal and vertical root mean square beam sizes $\sigma_x$ and $\sigma_y$ at a given location in the synchrotron as follows:

$$\sigma_x = \left(\beta_x \, \varepsilon \left(\frac{m_p c}{p}\right) + \left(\eta \, \frac{\sigma_p}{p}\right)^2\right)^{1/2} \qquad \text{1a}$$

$$\sigma_y = \left(\beta_y \, \varepsilon \left(\frac{m_p c}{p}\right)\right)^{1/2} \qquad \text{1b}$$

where the normalized emittance $\varepsilon$ is assumed to be the same in both planes, $p$ is the nominal proton momentum, $\sigma_p$ is the rms momentum spread, $m_p$ is the rest mass of the proton, and the second term in the brackets is absent in the vertical case because the vertical dispersion is zero. In other words, the transverse size of the proton beam varies around the PTA in proportion to the quantities plotted in Figure 3.2. ~~To determine the expected beam sizes,~~ the values of normalized emittance and momentum spread shown in Table 3.1 have been used. These values are based on actual Fermilab measurements adjusted to reflect the improved performance of modern linacs, as discussed in Section 2. Since the maximum beta function is approximately 4.0 meters in the horizontal and 5.8 meters in the vertical and the maximum dispersion function is approximately 2.6 meters, then the maximum expected horizontal and vertical rms beam sizes at injection time are 4.8 and 5.7 millimeters, respectively. It is readily seen that the contribution of the transverse emittance to the beam size dominates that of the momentum spread.

The straight sections in the PTA lattice are dispersionless. This is achieved by setting the horizontal betatron phase advance per cell to be very close to 90 degrees, so that the net phase

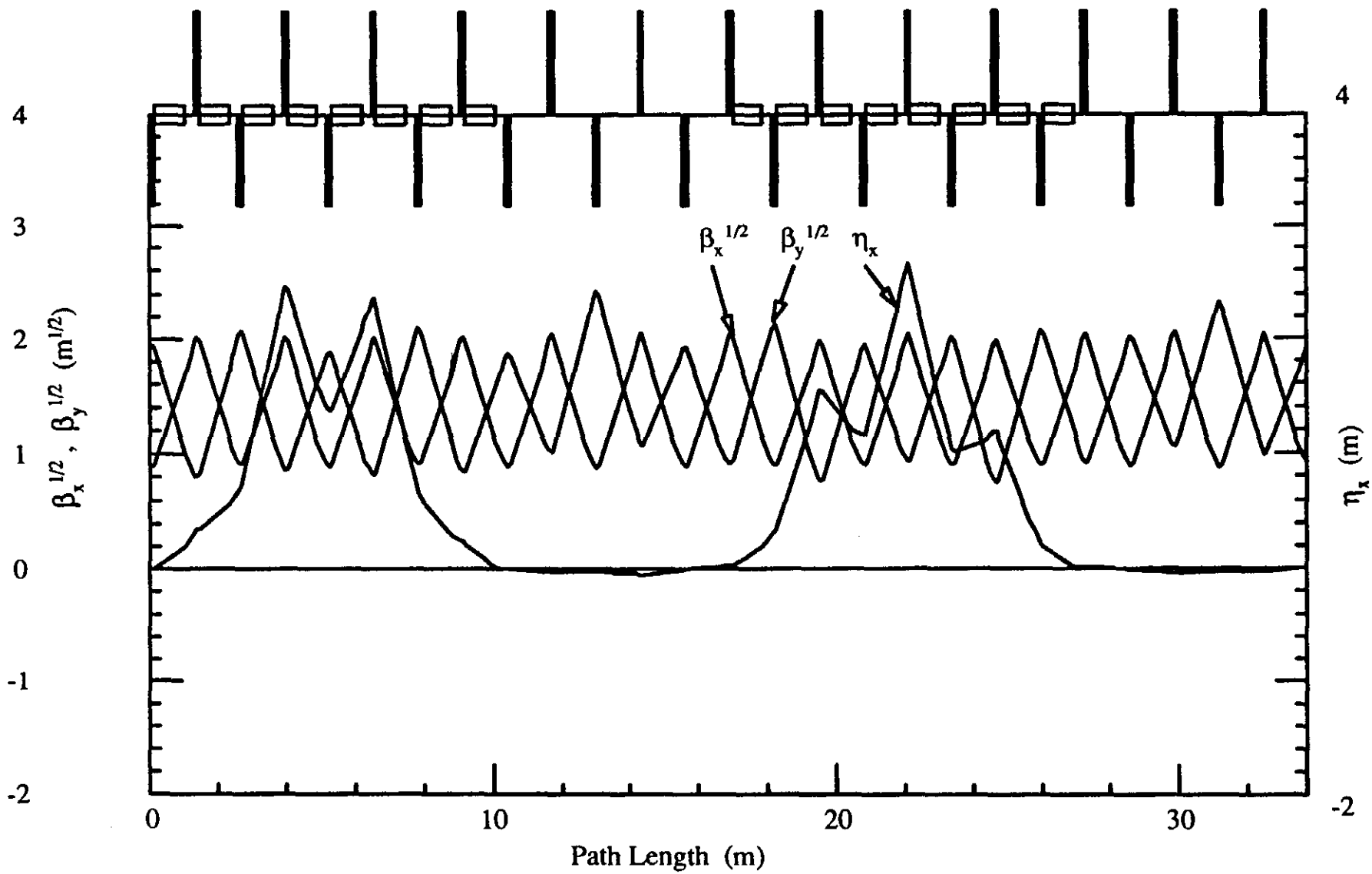


Figure 3.2 Optical functions and layout of the PTA synchrotron

advance per arc is 360 degrees. Of course, straight sections are included to accommodate various necessary functions such as injection, extraction, and acceleration, and these functions are simpler to implement and also work better in the absence of dispersion. The allocation of straight section space in the PTA is simple: two adjacent half-cells on each side are occupied by rf cavities, and each side has a fast kicker and a septum magnet separated by an empty half-cell reserved for future additions. One side of the ring is used for injection and the other for extraction.

Since the dipoles are rectangular, their pole face rotations focus the beam only in the vertical plane and not in the horizontal. This means that the horizontal phase advance in the straight cells is the same as in the bending cells, so that the total horizontal tune is approximately 3.25 . It also means that the vertical tune would be approximately 0.8 tune units higher if the focusing (F) and defocusing (D) quadruples were of the same integrated strength. In the present design, the vertical tune has been set (approximately) equal to the horizontal tune by varying the F and D quadrupole strengths independently. This can be achieved in practice, with identical quadrupoles, by allowing for two different current taps.

One power supply is used to drive all the dipoles and quadrupoles. As is customary with rapid-cycling synchrotrons, the magnets comprise the inductive part of an LC circuit driven at its resonant frequency, which is the same as the repetition rate $f_{rep}$ of the synchrotron. It is probably also possible to include the sextupoles on the main power supply. This power supply puts out a sinusoidal AC current added to a DC current bias so that the momentum of the beam as a function of time, p(t), which is simply proportional to the current, is given by

$$p(t) = \frac{p_{max} + p_{min}}{2} - \frac{p_{max} - p_{min}}{2} \cos(2\pi f_{rep} t). \qquad 2$$

In this expression injection occurs at t = 0 when $p = p_{min}$, and the beam occupies the ring only during the rising portion of the magnet ramp. The LC circuit of course involves energy storage alternately in the magnets and the capacitors, with the important advantage that the power consumption is greatly reduced - only dissipative losses need to be replaced, and there is no power-hungry flat-top in the magnet excitation curve. This technique has been successfully used for more than two decades, for example at the Cornell electron synchrotron (60 Hz) and at the Fermilab proton booster (15 Hz). Variation of the extraction energy is achieved in the PTA simply by adjusting the extraction time. This avoids the use of energy degraders, delivering higher quality beam with better resolution, but it does not avoid the need to change the excitation of the transport line magnets in proportion to the extraction momentum. However, the transport lines can be made rather insensitive to momentum matching errors by making them dispersion free - see below.

Rapid cycling synchrotrons present two design challenges. The first is the fact that conventional solid metal vacuum chambers cannot be used inside the dipoles, because the effects of the eddy currents induced during the ramp would be far too strong. A ceramic beam pipe is a reasonable solution for the quadrupoles and perhaps also for the dipoles. Another option that is used in practice at Cornell and at Fermilab is to put the vacuum chamber around the outside of the dipole. Another option is to use hybrid construction vacuum chambers that only allow current to flow along the direction of the beam, thereby allowing beam image currents to flow but not eddy current loops. The second design challenge is that the specifications of the radio frequency acceleration system become more significant, as discussed in the next section. It is shown there that the scope of the acceleration system is not unreasonable.

## 4. Radio Frequency acceleration system

The time rate of change of the beam momentum determines the required energy gain per turn $\Delta E$ and hence the accelerating voltage which the rf system must supply, according to:

$$\Delta E = 2\pi R \frac{dp}{dt}, \qquad 3$$

where R is the average radius of the machine and the rate of change of beam momentum is found by differentiating Equation 2:

$$\frac{dp}{dt} = \pi f_{rep} (p_{max} - p_{min}) \sin 2\pi f_{rep} t. \qquad 4$$

Naturally, a rapid-cycling machine requires more accelerating voltage than would a slow-cycling machine, but the maximum is only 6.8 kV for the PTA because the peak beam energy is low by the standards of high-energy accelerator laboratories. Thus the cost impact of the rf system is modest, providing further support for the notion that a rapid-cycling machine is the appropriate choice for proton therapy.

There are a number of reasons for choosing a harmonic number of one, that is, for setting the rf frequency equal to the beam revolution frequency and accelerating a single bunch. The linac beam pulse can then easily be injected into an already established bucket in the synchrotron, obviating the need for adiabatic capture. The beam does not then debunch after injection, so diagnostics such as beam position monitors which sense the rf structure of the beam do not experience a period when the beam signal disappears. Furthermore, the intensity can be adjusted over a wide dynamic range simply by changing the length of the linac beam pulse; straightforward and accurate control of the beam intensity is necessary in order to create uniform distributions when scanning the beam over a tumor, particularly for depth scanning. Operating with just one

bunch also facilitates extraction: a long beam gap occurs naturally to accommodate the rise time of the extraction kicker. Finally, it is unlikely that there will be coupled-bunch problems!

In order to provide phase stability, the beam must be accelerated at a synchronous phase of less than 90 degrees because the PTA is always below transition energy. The synchronous phase rises from zero at injection time to a maximum of about 47 degrees in the middle of the accelerating cycle, the time when the rate of change of momentum is fastest. The ring voltage peaks at about 9 kV at the same time.

Table 4.1 shows rf-related parameters.

| Property | units | Value |
|---|---|---|
| Harmonic number | | 1 |
| RF frequency at 15 MeV injection | MHz | 1.6 |
| RF frequency at 300 MeV extraction | MHz | 5.9 |
| Maximum total voltage | kV | 9.0 |
| Maximum accelerating voltage | kV | 6.8 |
| Maximum synchronous phase | degrees | 47 |
| Number of cavities | | 4 |
| Longitudinal emittance (total) | eV-sec | 0.02 |
| Maximum Laslett space charge tune shift | | 0.05 |

Table 4.1 Parameters for the Radio Frequency acceleration system in the PTA synchrotron.

Figure 4.1a shows the time dependence during the accelerating cycle of several rf-related parameters. The curve labeled K shows the variation of kinetic energy from 15 MeV to 300 MeV corresponding to the momentum dependence given by Equation 2. The curve labeled Frf shows the rf frequency rising from 1.6 MHz to 5.9 MHz during the cycle as it tracks the beam velocity for harmonic number h=1. The curve labeled Vrf shows the total ring voltage. The curve labeled A shows the bucket area rising monotonically from a value that matches the longitudinal emittance of

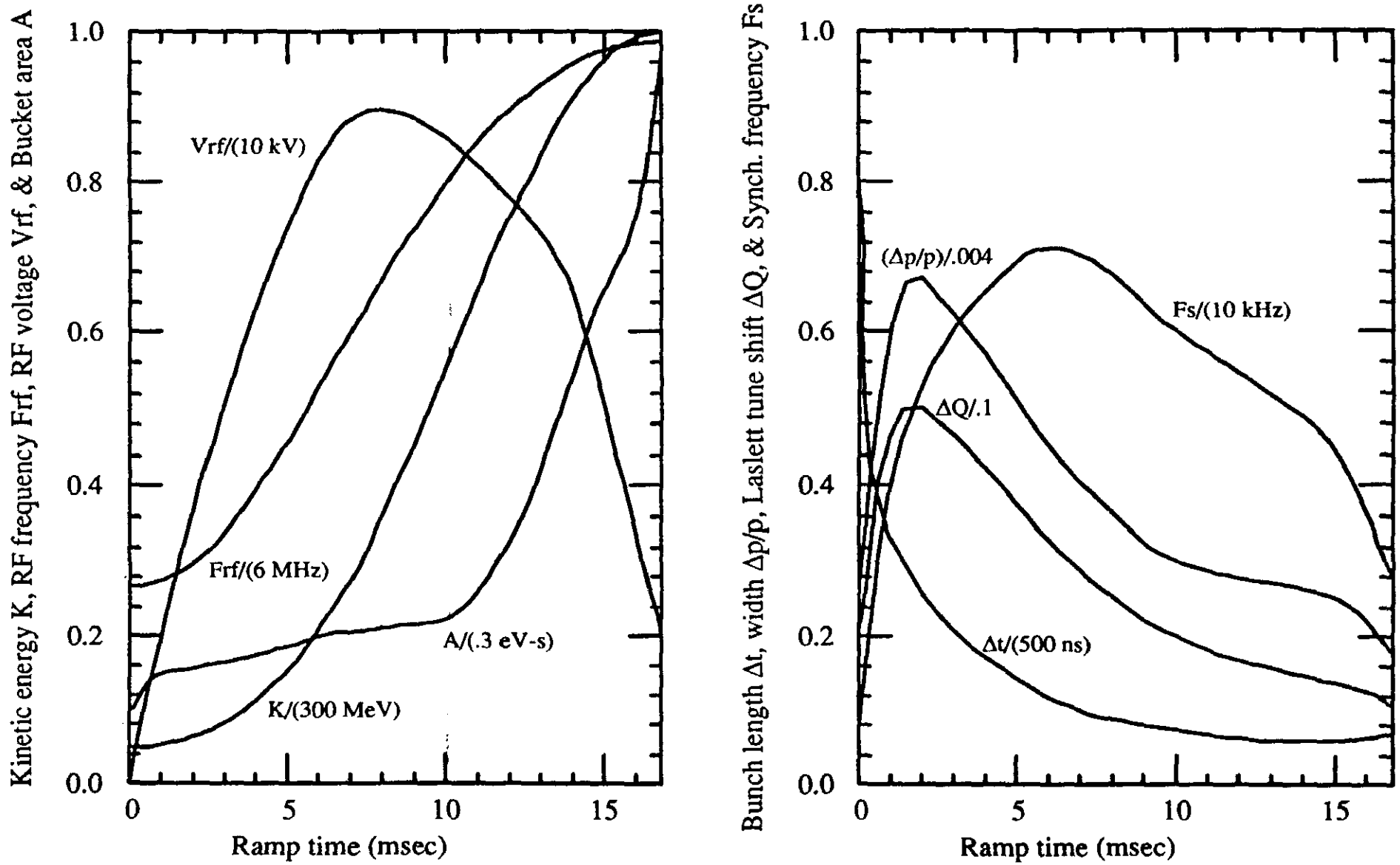


Figure 4.1 Radio Frequency acceleration parameters during a simulated 30 Hz ramp to 300 MeV

the incoming beam; indeed, the rf voltage curve was calculated to provide such a monotonic increase.

Figure 4.1b shows the time dependence of several additional rf-related parameters. The synchrotron frequency Fs starts out below 1 kHz and rises to about 7 kHz before tapering off toward the end of the cycle. $\Delta p/p$ is the total fractional momentum spread of the beam, and $\Delta t$ is the bunch length in nsec, calculated for a longitudinal phase space area of 0.02 eV-sec. The curve labeled $\Delta Q$ represents the magnitude of the Laslett space-charge tune shift for a beam of $10^{10}$ protons per cycle and rms normalized transverse emittances of 1 μm. It peaks at 0.05, well below the limit of about 0.3 suggested by experience with other proton synchrotrons.[9] As a result, no intensity-dependent space-charge effects are to be expected.

There are four rf accelerating cavities easily capable of providing 3 kV apiece. Since the required ring voltage is 9 kV, there is redundancy: the synchrotron can continue to operate at full energy while one of the four systems awaits repair. This kind of redundancy has made a valuable contribution to the beam availability at Fermilab.

The rf cavities are similar in design to the low-frequency cavities developed for the AGS Booster.[10] Each cavity is a simple ferrite-loaded cylindrical structure one meter long and about 40 cm in diameter with a central accelerating gap. The high-μ ferrite (TDKS7) comes in the form of toroids having inner and outer diameters of 10 cm and 30 cm, respectively. The cavities are tuned by biasing the ferrite from $\mu = 1100$ at 1.6 MHz to $\mu = 80$ at 6.0 MHz. The final power amplifier tube could be an Eimac 4CW25000B, which can deliver more than 25 kW of CW power.

# 5. Beam delivery and patient treatment planning

This section commences with general considerations about beam delivery and patient treatment planning and then describes specific beam delivery concepts. Delivery of beam to the patient is the area most likely to be affected by input from the medical professionals who will be the end users of the facility as well as by specific site constraints; thus at the pre-conceptual design stage it is appropriate (for both the designers and the design!) to exhibit considerable flexibility.

The beam delivery system comprises the hardware components and the associated software to control the beam trajectories downstream of the extraction septum. The initial complement of therapy facilities consists of two primary beamlines to deliver the proton bunches to one of two patient treatment areas. The first, and simplest, directs the beam to a tumor in a patient who is either standing (and supported) or sitting. (The Neutron Therapy Facility at Fermilab has considerable successful experience with treatment of patients in these orientations.) Horizontal and

vertical lateral scans are controlled with steering dipoles, while control of the beam entrance direction is accomplished by rotating the patient about a vertical axis. The second, more complicated, line directs the beam to an isocentric gantry which rotates around a reclining patient, somewhat like the arrangement used at Loma Linda. This gantry system, which involves a total of 360 degrees of bending, is provided for those situations where treatment in a roughly vertical orientation is deemed inappropriate. It is larger, more expensive, and harder to set up and maintain than the roughly horizontal beam. Patients for whom the simpler horizontal beam is appropriate would reap the benefits of faster and less costly treatment.

### Treatment planning

As has been pointed out previously, a rapid-cycling synchrotron enables a precise digital approach to therapeutic dose delivery. The goals of patient treatment planning are conceptually simple: to deliver the intended dose to the treatment volume while minimizing damage to normal tissue and avoiding damage to critical anatomical structures. However, achieving these goals in a realistic three-dimensional situation of an irregularly shaped tumor surrounded by anatomical structures of variable density and composition is a challenge to computing and control systems. Therefore, fully realizing the potential of proton therapy requires an integrated approach to medical imaging, patient treatment planning in three dimensions, patient localization, and control of accelerator and beam delivery systems using state-of-the-art computing techniques. Digital dose delivery holds the most promise for achieving these goals.

Treatment planning will be based on computer calculations and modelled on existing planning programs such as those used at Massachusetts General Hospital, the University of Wisconsin, and Loma Linda University Medical Center. Necessarily, there will be modifications, as "pointillism," the tumor scanning strategy to be employed, is conceptually different from those used elsewhere. Patient alignment and control will be accomplished using a laser-based feedback system like the one already in use at Fermilab's Neutron Therapy Facility. Normal procedures will include regular recalibration of these controls.

### Patient safety

A rapid-cycling synchrotron also lends itself to a simple, reliable approach to patient safety; indeed, we perceive this to be one of its main virtues. Conditions will be monitored on each cycle; if dangerous abnormal conditions are detected, any beam currently in the synchrotron will be aborted and subsequent cycles will be inhibited at the source. An abort system internal to the synchrotron is probably most appropriate. Two dipoles separated by 180 degrees of phase advance in one of the arcs can be pulsed to sweep the beam into an absorber block halfway

between them. The trigger to the extraction kicker would simultaneously be inhibited. Examples of situations which would produce this response include an unexpectedly large proton bunch intensity, out of tolerance orbit fluctuations, errors in gantry or patient alignment, or a hardware failure in the final beam steering system. Detection of alarm conditions will require continuous monitoring of beam position and circulating-beam intensity monitors. The final intensity monitor will also serve to log beam delivery automatically for the patient's records. The record will contain pulse-by-pulse information of exposure and orientation so that dosages can be reconstructed in complete detail.

One can imagine rare but perhaps not impossible failure modes which conspire to circumvent such monitoring systems. A great safety advantage of using a rapid-cycling synchrotron is that the maximum single bunch intensity is too low to cause serious damage even if a single bunch goes astray and strikes the patient in an unexpected way. As a last line of defense in a multi-layered approach to patient safety, monitors just upstream of the patient will detect the first such out-of-tolerance bunch, and the beam will be inhibited at the source on subsequent cycles until the situation is understood, which might well entail removing the patient from the treatment position and operating the system with a suitable phantom in place of the patient. Our goal is to provide safe, precise, effective, thoroughly monitored treatment using highly reliable, easily maintained (or replaced) hardware.

### Beam transport line

Figure 5.1 shows the schematic layout of a horizontal beam delivery line that extracts protons from the PTA synchrotron and delivers them over approximately 36 meters (a distance that is easily adjusted) to the patient. The figure shows the behavior of the optical functions in one configuration of the entire line, and shows how it is naturally broken down into four subsections that are discussed more or less sequentially below. They are

i) the achromatic "extraction" section,

ii) the "lengthener" that joins nominal length half cells to long half cells,

iii) the variable length "transport" section, and

iv) the variable focus "nozzle".

Table 5.1 lists various parameters appropriate to the delivery line.

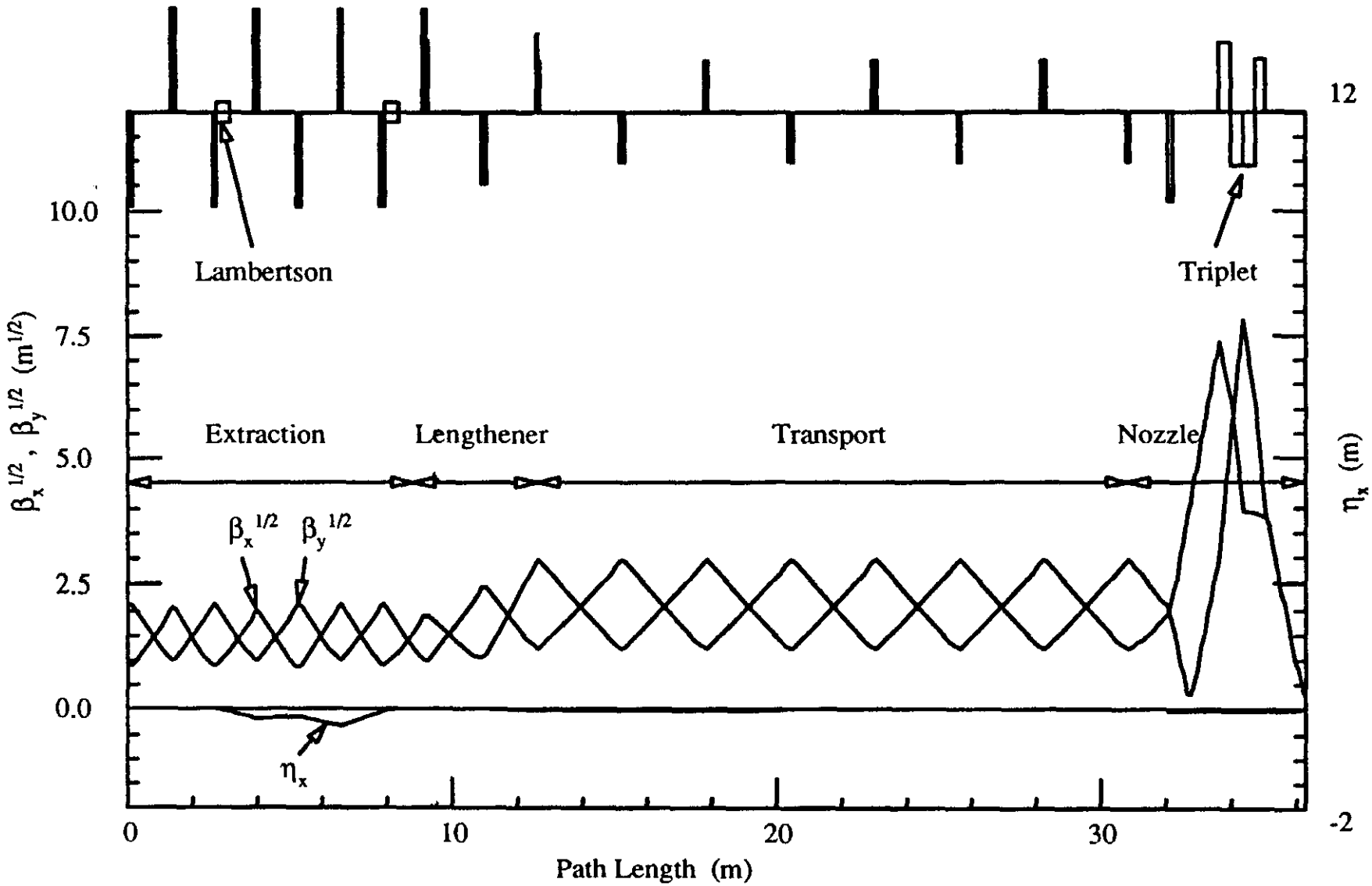


Figure 5.1 Optical functions and subsections of the delivery line

| Property | units | Value |
|---|---|---|
| Kicker bend angle | radians | 0.006 |
| Lambertson bend angle | radians | 0.178 |
| Magnetic length of Lambertson | m | 0.4 |
| Maximum Lambertson field | Tesla | 1.2 |
| Length of transport line half cells | m | 2.6 |
| Length of nozzle quadrupole Q4 | m | 0.2 |
| Length from Q4 to triplet | m | 1.4 |
| Length of nozzle quadrupole Q3 | m | 0.36 |
| Length of nozzle quadrupole Q2 | m | 0.72 |
| Length of nozzle quadrupole Q1 | m | 0.36 |
| Total length of nozzle triplet | m | 1.44 |
| Distance from nozzle to patient (beam focus) | m | 1.2 (variable) |

Table 5.1 General parameters of the horizontal delivery line and the beam focusing nozzle.

Again it should be emphasized that the design presented here is pre-conceptual, and has not undergone final optimization of parameters. For example, the actual length of the long half cells would probably not be exactly twice the PTA half cell length in practice.

There are five empty half cells in the injection and extraction straights of the PTA synchrotron. The first two half cells of the extraction section presented here are the same two half cells that begin the extraction straight in the synchrotron, starting with a D quadrupole. Immediately after the D quadrupole is a fast kicker that deflects the beam vertically by a small angle of approximately 6.0 milliradians. This causes the beam to be displaced by about 2.4 centimeters at the location of a horizontally bending Lambertson septum magnet one cell downstream. A full-energy kicked beam experiences a field of about 1.2 Tesla in the 0.4 m long Lambertson, giving it a horizontal angle of approximately 0.178 radians, and displacing the beam horizontally by 17.0 centimeters at the next quadrupole downstream. The extracted beam is

physically separate from the PTA at this stage but is still traveling in a FODO cell structure like that of the ring. Quadrupoles in the extraction subsection could be run on the main power supply.

Both the horizontal and the vertical extraction angles launch dispersion waves in the transport line, but the vertical dispersion is negligibly small. The horizontal dispersion wave can be canceled by placing a dipole with the same bend angle as the Lambertson $4N + 2$ full cells downstream, where $N$ is any integer, or by placing an equal and opposite bend $4N$ full cells downstream. In the case presented here, a bend of the same polarity is placed 2 full cells downstream, about 5.2 meters downstream from the extraction Lambertson. It is easy to see how a "switchyard" consisting of several such dipoles can be constructed, so that as many dispersion-free transport lines as desired can be served. As long as an adequate amount of space is reserved in the first place, the ability to add treatment lines in the future is guaranteed.

Short half cells are desirable in the synchrotron since the beta functions are proportionally small, leading to tighter focusing and a smaller beam (see Equation 1). This, in turn, allows magnets with smaller apertures and hence smaller transverse dimensions in general. In other words, the closer the spacing of the synchrotron quadrupoles, the smaller, lighter, and cheaper are both the dipoles and the quadrupoles. This argument needs modification for the proton delivery lines, where not many dipoles are necessary and the desire is to reduce both the number of quadrupoles and the power consumption necessary to reach the treatment rooms. Since the beam size goes down with increasing momentum, the tightness of the focusing can be relaxed while using the same quadrupoles by spacing them further apart.

Quadrupoles in the "transport" subsection are placed twice as far apart as normal, for a half cell length of 2.6 meters. Because of this, the beta functions are twice as large, and the beam size is $\sqrt{2}$ times as large (at the same momentum). Since the same length quadrupoles are used as elsewhere, their excitation current is halved. So there are half as many quadrupoles per meter of transport distance, and the power requirement for an individual quadrupole is one quarter of nominal. Hence the power per meter is one eighth of the power that would be required if the nominal half cell length were used. The price paid for this, aside from the slightly increased transverse beam size, is the necessity to connect the "extraction" subsection to the "transport" subsection with optical grace.

The "lengthener" subsection of the transport line smoothly matches the optical functions of nominal length "extraction" FODO cells to the double length "transport" FODO cells. If this were done abruptly - for example, if the "lengthener" were simply omitted - then the beta functions would not undulate in the regular fashion shown in Figure 5.1, but would fluctuate significantly.

The height of a box representing a quadrupole in Figure 5.1 is proportional to the strength of that quadrupole, showing that the three "lengthener" quadrupoles each have different strengths that are neither the strength of the "extraction" quadrupoles nor the single strength of the "transport" quadrupoles. These three quadrupoles must have separate power supplies or shunts.

### The "nozzle"

The "nozzle" consists of the final four quadrupoles that adjust the beta functions immediately before delivery to the patient. This arrangement, patterned after the so-called low-$\beta$ insertions that are used to control the beam size at the center of high energy physics experiments in hadron colliders[11], provides extremely flexible optics. Quadrupole Q4, farthest from the patient, is approximately 1.3 meters - half of the half cell length - from the last "transport" quadrupole. This is followed, in the typical scenario presented here, by a 1.4 meter long drift, before encountering the closely packed triplet of quadrupoles, Q3-Q2-Q1, after which comes a final drift of 1.2 meters to the focal point at the tumor in the patient. The distance from the inner face of Q1 to the patient is not crucial to this scheme - it can be reduced or increased significantly, as desired.

Figure 5.2 shows a close-up of the optical performance of the nozzle when the beta function at the patient, $\beta_{patient}$, is adjusted over three orders of magnitude, from 0.1 to 100 meters, demonstrating the extreme flexibility of the optical system. In the absence of multiple scattering in the patient, this is equivalent to beam spot sizes varying from 0.34 to 10.8 millimeters at 300 MeV. Recall that the quantities plotted, $\sqrt{\beta}$ in both planes, are proportional to the transverse sizes of the beam. When $\beta_{patient}$ is very small, the beam is strongly convergent, significantly reducing the entrance radiation dose. However, the smallest practical beam size is limited by multiple scattering, so that such sharp focusing is not very advantageous except for shallow problems such as ocular tumors. When $\beta_{patient}$ is very large, the practical limit to the maximum size of the beam is the aperture of the triplet quadrupoles. In this configuration the beam is not convergent at all but is essentially parallel. Note that in no case can the beam be considered to be coming from a point source; hence there is no inverse-square augmentation of entrance dose.

Table 5.2 shows the excitations of the four nozzle quadrupoles, as measured by the slope of the B-field, in the four configurations shown in Figure 5.2. The table shows that quadrupoles Q1 and Q4, which undergo the largest variations, must have separate power supplies. It may be possible to power quadrupoles Q2 and Q3 using a single power supply and a shunt. If the maximum acceptable quadrupole pole tip field is 1.0 Tesla when the field gradient is 14.2 Tesla per meter, then the pole tip radius of the triplet quadrupoles must be less than 7.0 centimeters.

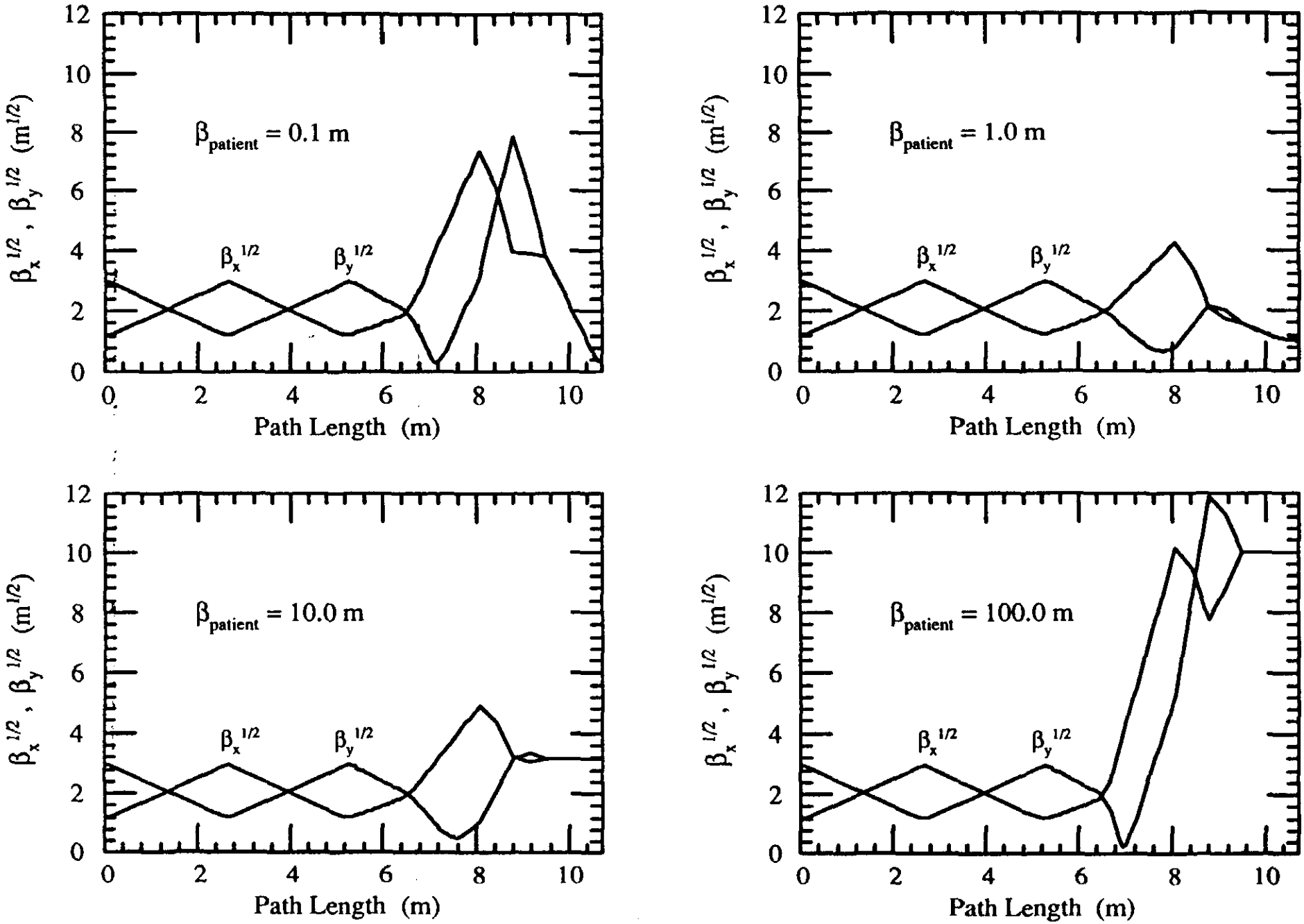


Figure 5.2 Optical functions in four configurations of the nozzle

This is much larger than the largest beam size of 1.6 centimeters that occurs when the beams are essentially parallel, so that the beam has the same size in the triplet as in the patient.

| $\beta_{patient}$ (m) | 0.1 | 1.0 | 10.0 | 100.0 |
|---|---|---|---|---|
| Focal spot size @ 70 MeV (mm) | 0.50 | 1.59 | 5.04 | 15.9 |
| Focal spot size (mm) | 0.34 | 1.08 | 3.41 | 10.8 |
| Gradient of Q1 (Tesla/m) | 10.9 | 3.7 | 1.8 | 5.3 |
| Gradient of Q2 (Tesla/m) | 11.1 | 8.9 | 6.0 | 7.1 |
| Gradient of Q3 (Tesla/m) | 14.2 | 13.0 | 10.4 | 10.5 |
| Gradient of Q4 (Tesla/m) | 18.5 | 4.9 | 7.9 | 29.8 |

Table 5.2 Four focusing configurations of the nozzle. The spot sizes quoted do not include the effects of multiple scattering. Except for the first row of the table, all values are quoted for a kinetic energy of 300 MeV.

Large apertures are desirable in the triplet quadrupoles, however, when large tumors are being treated. When $\beta_{patient}$ is large, and the beam is wide and parallel, then horizontal and vertical dipole steering magnets placed close to Q4 are used to move the beam transversely by the same amount at the patient and in the bore of the triplet. When the beam is scanned uniformly in this way, the integrated dose delivered to the patient is the same as if it came from a very large stationary parallel beam. That is, the largest tumor that can be treated, before having to worry about enhanced inverse square deposition at the surface of the patient, is a tumor that is the same size as the bore diameter of the triplet quadrupoles. Tumors as big as 14.0 centimeters are easily treated in the scenario presented above.

The caveat that the designs presented here are pre-conceptual applies a fortiori to the foregoing discussion of the nozzle. For example, a realistic triplet design must include longitudinal space between the component quadrupoles, whose lengths can clearly be modified from the simple 1:2:1 ratios used here.

# Acknowledgements

We learned osmotically about the benefits of proton therapy and the pros and cons of various therapy designs from Fermilab colleagues too numerous to mention who worked on the Loma Linda synchrotron. We are grateful for significant interactions with Frank Hendrickson, Michael Goitein, George Chen, Franca Kuchnir, Ken Hanson, Rol Johnson, and Ken Thomas on a variety of topics related to proton therapy. During the course of frequent discussions, Arlene Lennox contributed to the development of this design by providing important information about medical requirements on a therapy facility. Bill Miller and Dave Wildman contributed specific ideas about rf systems to this design. Encouragement from John Peoples, the Director of Fermilab, and from Steve Holmes, the Head of the Accelerator Division, is much appreciated.

# Footnotes and References

*Operated by the Universities Research Association, Inc. under contract with the U.S. Department of Energy.

1. R. R. Wilson. "Radiological use of fast protons." Radiology, 47:487, 1946.

2 E.S.Gragoudas, et al., Opthalmology vol.87, 571 (1980); J.M.Slater, D.W.Miller, and J.O.Archambeau, Int. J. Radiation Oncology Biol. Phys. vol.14, 761 (1988) and references therein. The PTCOG Newsletter edited by Janet Sisterson sometimes updates the statistics.

3. M. Goitein, "Clinical Specifications for a Charged Particle Medical Facility", Proceedings of a Medical Workshop on Accelerators for Charged-Particle Beam Therapy, Fermilab, January 1985.

4. F. T. Cole. "Accelerator considerations in the design of a proton therapy facility - a reprise." Technical report. Particle Accelerator Corporation. 4513 Cornell Avenue, Downers Grove, IL 60515. August 23, 1991.

5. Eros Pedroni, Reinhard Bacher, Hans Blattmann, Terence Boehringer, Adolf Coray, Mark Phillips, and Stefan Scheib, "Cancer therapy with 200 MeV protons at PSI. Development of a fast beam scanning method and future plans for a hospital based facility." Presented at the 1990 European Particle Accelerator Conference.

6. S. Fukumoto et al. "Present status and future of University of Tsukuba Proton Medical Research Center." Presented at the National Institute of Radiological Science International

Workshop on Heavy Charged Particle Therapy and Related Subjects (NIRS: Chiba 260, Japan). July 4-5 1991. See also Sadayoshi Fukumoto, "A dedicated accelerator for proton therapy at Tsukuba." Contributed to the 4th China-Japan Joint Symposium on Accelerators for Nuclear Science and their Applications (Beijing, China). October 15-17 1990.

7. K.M. Hanson, J.N. Bradbury, T.M. Cannon, R.L. Hutson, D.B. Laubacher, R.J. Macek, M.A. Paciotti, and C.A. Taylor, "Computed tomography using proton energy loss", Phys. Med. Biol., 1981, Vol. 26, pp 965-983. K.M. Hanson, J.N. Bradbury, R.A. Koeppe, R.J. Macek, D.R. Machen, R. Morgado, M.A. Paciotti, S.A. Sandford, and V.W. Steward, "Proton computed tomography of human specimens", Phys. Med. Biol., 1982, Vol. 27, pp 25-36.

8. E. Tanke, M. Vretenar and M. Weiss, "Performance of the CERN High-Intensity RFQ." Proc. 1990 Linear Acc. Conf., Albuquerque, NM, p. 686.

9. Steven M. Stahl, "Beam Dynamics in the Fermilab Booster in the Presence of Space Charge", Northwestern University Ph.D. thesis, June, 1991.

10. R. T. Sanders, P. Cameron, W. Eng, M. Goldman, D. Kasha, A.J. McNerney, M. Meth, A. Ratti, and R. Spitz, "The AGS Booster low frequency RF system", Conference Record of the 1991 IEEE Particle Accelerator Conference, San Francisco, p. 739.

11. S. Peggs, "Accelerator physics issues in large proton storage rings." Technical Report SSC-85. SSC Central Design Group. Lawrence Berkeley Laboratory. August, 1986. Submitted to the 13th International Conference on High Energy Accelerators. Novosibirsk, USSR. August 7-11, 1986.